View metadata, citation and similar papers at core.ac.uk

brought to you by CORE

provided by WestminsterResearch

UNIVERSITY OF FORWARD THINKING WESTMINSTER

WestminsterResearch
http://www.westminster.ac.uk/westminsterresearch

# Mass Univariate Regression Analysis for Three-Dimensional Liver Image-Derived Phenotypes

**Thomas, E.L., Thanaj, M., Basty, N., Liu, Y., Cule, M., Sorokin, E., Thomas, E.L., Bell, J.D. and Whitcher, B.**

This is an author's accepted manuscript of an article published in Papież B.W., Yaqub M., Jiao J., Namburete A.I.L., Noble J.A. (eds) Medical Image Understanding and Analysis. MIUA 2021. Lecture Notes in Computer Science, vol 12722. Springer, Cham. https://doi.org/10.1007/978-3-030-80432-9_13.

The final authenticated publication is available at Springer via:

https://doi.org/10.1007/978-3-030-80432-9_13

The WestminsterResearch online digital archive at the University of Westminster aims to make the research output of the University available to a wider audience. Copyright and Moral Rights remain with the authors and/or copyright owners.

# Mass Univariate Regression Analysis for Three-Dimensional Liver Image-Derived Phenotypes

Marjola Thanaj[1][0000−0002−1789−7112], Nicolas Basty[1][0000−0002−1330−0913], Yi Liu[2][0000−0003−2745−6940], Madeleine Cule[2][0000−0002−7400−5643], Elena P. Sorokin[2][0000−0001−8957−8869], E. Louise Thomas[1][0000−0003−4235−4694], Jimmy D. Bell[1][0000−0003−3804−1281], and Brandon Whitcher[1][0000−0002−6452−2399]

[1] Research Centre for Optimal Health, School of Life Sciences, University of Westminster, London, UK
m.thanaj@westminster.ac.uk
[2] Calico Life Sciences LLC, South San Francisco, California, USA

**Abstract.** Image-derived phenotypes of abdominal organs from magnetic resonance imaging reveal variations in volume and shape and may be used to model changes in a normal versus pathological organ and improve diagnosis. Computational atlases of anatomical organs provide many advantages in quantifying and modeling differences in shape and size of organs for population imaging studies. Here we made use of liver segmentations derived from Dixon MRI for 2,730 UK Biobank participants to create 3D liver meshes. We computed the signed distances between a reference and subject-specific meshes to define the surface-to-surface (S2S) phenotype. We employed mass univariate regression analysis to compare the S2S values from the liver meshes to image-derived phenotypes specific to the liver, such as proton density fat fraction and iron concentration while adjusting for age, sex, ethnicity, body mass index and waist-to-hip ratio. Vertex-based associations in the 3D liver mesh were extracted and threshold-free cluster enhancement was applied to improve the sensitivity and stability of the statistical parametric maps. Our findings show that the 3D liver meshes are a robust method for modeling the association between anatomical, anthropometric, and phenotypic variations across the liver. This approach may be readily applied to different clinical conditions as well as extended to other abdominal organs in a larger population.

**Keywords:** Registration · Surface-to-Surface · Morphology · Magnetic Resonance Imaging.

## 1 Introduction

Magnetic resonance imaging (MRI) has become the benchmark for clinical research in the study of body composition, particularly for measurements of visceral adipose tissue, liver and pancreatic fat content. The incidence of chronic

conditions such as type-2 diabetes, cardiovascular disease and non-alcoholic fatty liver disease are rising rapidly, which reflects the increasing prevalence of obesity in society [27]. Organ and tissue MRI measurements, referred to as image-derived phenotypes (IDPs) have the potential to enhance our understanding of the precise phenotypic changes underlying these conditions [25].

The UK Biobank is a population-based prospective study that has recruited over 500,000 volunteers, aged 40–69 years old, with the goal of advancing our understanding of health and disease [10]. A subset of 100,000 participants has been invited for a medical imaging assessment that includes a standardised abdominal acquisition protocol. The UK Biobank abdominal imaging protocol produces several MRI datasets that focus on basic structure and composition measurements in the thorax, abdomen and pelvis [16]. Specifically, the abdominal protocol includes a two-point Dixon sequence [12] with neck-to-knee coverage, as well as a multiecho single-slice acquisition of the liver. This latter acquisition enables non-invasive estimation of tissue composition including proton density fat fraction (PDFF) and iron concentration. Together these sequences enable accurate, quantitative analysis of multiple liver IDPs.

Performing semantic segmentation on abdominal organs using deep learning methodology is now widely established. The basic IDP obtained from organ segmentation is total volume, a single number that is informative but does not capture the complex morphology of the underlying physical structure of an organ. Computational image analysis, by which machine learning is used to annotate and segment the images, is gaining traction as a means of representing detailed three-dimensional (3D) mesh-derived phenotypes related to shape variations at thousands of vertices in a standardised coordinate space. One approach to inference is to transform the spatially correlated data into a smaller number of uncorrelated principal components [4], while the modes from PCA are useful in exploratory data analysis they do not provide an explicit model relating 3D shape to other phenotypic measures. A more powerful approach may be to estimate parameters at each vertex of the 3D surface mesh, hence creating a so-called statistical parametric map (SPM), a concept widely used in functional neuroimaging [20] and cardiac imaging [9]. A recent study in the cardiovascular imaging domain, implementing a mass univariate framework, showed the ability of this technique in identifying interactions between genetic variation related to hypertrophic cardiomyopathy and a 3D cardiac phenotype [18]. On that note, scientific questions of interest, such as, how organ shape is associated with disease state (e.g., type-2 diabetes, cardiovascular disease, non-alcoholic fatty liver disease) or gene expression (e.g., a single-nucleotide polymorphism or SNP), may be quantified by selecting a cohort of cases and controls from an available population and including common covariates in a linear regression framework.

In this paper we extend techniques developed in neuroimaging and cardiovascular imaging fields to liver imaging by implementing a mass univariate framework that maps associations within the phenotypic variation. Such an approach would provide overly conservative inferences without considering spatial dependencies in the underlying data, so we evaluated threshold-free cluster-

enhancement with respect to liver phenotypes for the sensitive detection of coherent signals in order to understand their efficacy in identifying phenotypic interactions in liver shape and structure. A cohort of UK Biobank participants are analyzed using our methodology, with the aim to investigate the associations between both image-derived and non-image-derived phenotypes and local liver morphology and establish anatomical structures in the liver. We further explore the feasibility of SPMs in comparing groups of subjects using mesh-based shape analysis. These 3D derived morphometric phenotypes will significantly contribute to our understanding of the relationship between form and function in health and disease.

## 2 Materials and Methods

### 2.1 Data

In this work, we used liver segmentations predicted from the Dixon MRI acquisitions in the UK Biobank Imaging Study. The Dixon acquisition contains six separate series for each subject. We performed basic pre-processing to assemble the six series into a single volume [17]. Briefly, the six series were resampled to the same resolution ($2.23 \times 2.23 \times 3.0$ mm$^3$), bias-field correction was performed and the six series were blended together resulting in a final volume of size ($224 \times 174 \times 370$ voxels). Segmentations were performed using a convolutional neural network based on the U-net architecture [22], trained using 120 manual annotations performed by a team of radiographers. The segmentation model achieved a dice score coefficient of 0.932 in out-of-sample data [17].

For the mass univariate regression analysis, we randomly selected 2,730 participants from the UK Biobank Imaging Study to cover a broad range of age, gender and body compositions. Detailed descriptions of the full cohort can be found in the section below. A randomly selected sub-cohort of 20 participants (70% females; age range: 50-78 years; average age: 56.8 years) was used to construct the template liver mesh.

### 2.2 Image Analysis and Mesh Construction

Image registration was performed in two stages to construct the liver template: affine registration to account for translation, rotation, scaling and shearing, and non-rigid registration to account for local deformation using the symmetric image normalization (SyN) method with cross-correlation as the similarity metric [1,3]. The algorithm maps a group of images to a common space by finding the template and set of transformations with the lowest dataset parameterization. The size of the parameterization, here, is given by the SyN implementation which measures the image similarity metric and diffeomorphism maps [3]. Here, we performed the image registration with no initial template as input instead, the template is derived completely from twenty images. In particular, we transformed the liver segmentations of twenty subject-specific volumes to the template

space using the non-rigid transformation and computed a template in four iterations. This computes the Euclidean distance as a metric for average shape which corresponds to the average liver across all subjects. A surface mesh was then constructed from the average template using the marching cubes algorithm and Laplacian smoothing in the VTK library (Kitware Inc.), and a template was created in a coordinate space [5]. Fig. 1, illustrates a scheme summarising the pipeline for the template mesh construction.

Once the template was available we performed a registration step where all subject-specific segmentations were rigidly aligned to a template segmentation. The subject meshes were then constructed enabling the further computation of 3D mesh-derived phenotypes. The liver meshes encode the 3D mesh-derived phenotype variation for the study cohort, in particular, for each subjects' mesh, surface-to-surface (S2S) values were measured by computing the nearest-neighbour signed distance between the template surface and a subjects' surface for each vertex. After a manual quality control process investigating for outliers on the surface-to-surface values, all values were no larger than the range $\pm 65$ mm.

The template construction was performed using Advanced Neuroimaging Tools (ANTs) [1,2,3] using cross correlation (`CC`) as the similarity metric, the B-spline non-rigid transformation model (`BSplineSyN`) and default parameters otherwise. The subject's registration was performed using the rigid and affine transform type (`a`) and the rest of the default parameters from ANTs. The 3D mesh-derived phenotype was computed using the packages **FNN** [7] and **Rvcg** [23] in R 3.6.1 [21].

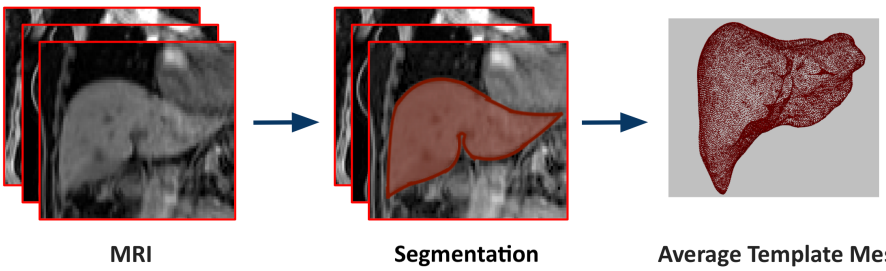


**Fig. 1.** Average template mesh construction. Dixon MRI volumes from UK Biobank abdominal protocol (left) are used to produce subject-specific 3D liver segmentations (middle), then images are registered to a common space and combined to produce an average template mesh.

### 2.3 Mass Univariate Regression Analysis

The association between the 3D mesh-derived phenotype and anthropometric variables is modeled using a linear regression framework. Given $n_s$ subjects from

a sample of the population under study, the linear regression model was expressed as

$$Y = X\beta + \epsilon, \tag{1}$$

where $Y$ is a $n_s \times n_v$ matrix containing ($n_v$ is the number of voxels in the mesh), for example, the S2S values of all the $n_s$ subjects at each vertex of the 3D liver mesh, $X$ is the $n_s \times p$ design matrix of $p$ known covariates (including the intercept) and the clinical variables for each subject, such as age and sex, used to model the hypothesis under investigation. $X$ is related with $Y$ by the vector of the regression coefficients $\beta$. In this way, $Y$ may be associated with each of the columns of $X$ adjusted for the other covariates. Finally $\epsilon$ is a $n_s \times n_v$ matrix which is independent and identical distributed across the subjects and is assumed to be a zero-mean Gaussian process [14]. The estimated regression coefficients $\hat{\beta}$ and their related $p$-values at each vertex in the mesh may be displayed on the whole 3D liver anatomy, providing the spatially-distributed associations. We applied threshold-free cluster-enhancement (TFCE) to enhance areas of the signal that exhibit spatial contiguity and better discriminate the estimated parameters between noise and spatially-correlated signal [9,24]. The mass univariate regression model for deriving associations between clinical parameters and a 3D phenotype is outlined in Fig. 2.

The TFCE statistic at each vertex $v$ of the 3D mesh under study is given by

$$\mathrm{TFCE}(v) = \int_{h=h_0}^{h_v} e(h)^E h^H dh, \tag{2}$$

where $h$ is the value of the corresponding $t$-statistic and is raised from zero ($h_0$) up to the height of the vertex $v$ ($h_v$), $e(h)$ is the extent of the cluster with threshold $h$ that contains $v$ vertices, and $E$ and $H$ are two hyperparameters empirically defined to be 0.5 and 2 [24].

The derived $p$-values were corrected to control the false discovery rate (FDR) using the Benjamini-Hochberg procedure [6] as it has been shown to provide the optimal $p$-values and areas of significance [9]. Together TFCE and permutation testing were applied to compute a new set of $p$-values at each mesh vertex $v$, by sampling the data and computing the TFCE $N$ times over the obtained statistical parametric maps. The permutation testing was performed to estimate the null distribution for the univariate statistics. In particular, we permuted the data $N$ times obtaining TFCE scores where the test statistics are summed forming a cluster mass statistic. The permutation testing identifies the largest cluster among those permutations [9]. Here, we used the Freedman-Lane technique as a permutation framework, as it provides powerful permutation and optimal control of false positives [13,26]. The mass univariate regression analysis was performed from a refined version of the package **mutools3D** [8] in R 3.6.1 [21].

## 3 Results

We analysed liver MRI data from 2,730 participants in UK Biobank from which 97.7% were Caucasian and aged between 46 to 80 years old. The main cohort

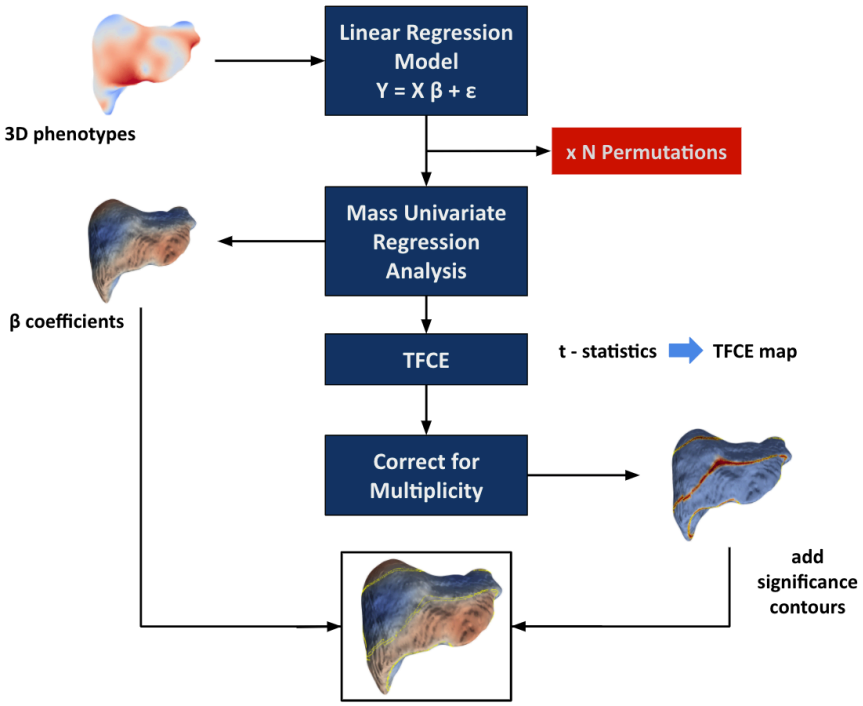


**Fig. 2.** Flow diagram for the mass univariate regression analysis of three-dimensional phenotypes. Phenotypes are used to construct the linear regression model, where mass univariate regression analysis produces parameter estimates ($\hat{\beta}$) and the null distribution via permutation. TFCE is applied to the $t$-statistics from the regression analysis to produce the significance threshold. The associated $p$-values are corrected for multiple comparisons and mapped on to the mesh for visualisation. This diagram was modified from [9].

characteristics are shown in Table 1. To assess the associations between S2S and anthropometric covariates as well as liver IDPs, we performed mass univariate regression analysis adjusting for age, sex, ethnicity, body mass index (BMI) and waist-to-hip ratio (WHR). The TFCE algorithm was applied to the $t$-statistics and on the permuted $t$-statistics ($N = 1,000$ times) for each analysis. Correction for multiplicity via the FDR was applied for the number of vertices and the number of anthropometric covariates/IDPs tested.

A summary of the regression models for the whole cohort, representing the significance area on the liver is shown in Table 2. S2S values is shown to increase with age with a positive association on 39 out of 57% of the significance area, while WHR and BMI showed a decline with increased S2S values. To determine the nature of the liver modeling we examined the effects of the liver IDPs such as iron concentration and PDFF. Liver iron was positively associated with S2S

**Table 1.** Baseline characteristics and liver IDPs. Values are presented as mean ± SD for continuous variables and counts for discrete variables.

| | Full Cohort | Men | Women |
|---|---|---|---|
| $N$ | 2,730 | 1,368 | 1,362 |
| $N$ Caucasian | 2,669 | 1,337 | 1,332 |
| Age (years) | 62.8 ± 7.2 | 63.4 ± 7.3 | 62.2 ± 7.1 |
| BMI (kg/m$^2$) | 26.3 ± 4.1 | 26.7 ± 3.9 | 25.8 ± 4.3 |
| WHR | 0.88 ± 0.09 | 0.93 ± 0.06 | 0.82 ± 0.07 |
| Liver Iron (mg/g) | 1.21 ± 0.26 | 1.22 ± 0.27 | 1.20 ± 0.24 |
| Liver PDFF (%) | 4.8 ± 4.7 | 5.6 ± 5.1 | 4.0 ± 4.1 |

values on 36% of vertices, and negatively associated on 2% of the vertices whereas liver PDFF showed a positive association on 48 out of 55% of the vertices.

**Table 2.** Significance areas for covariates in the mass univariate regression model. The significance area is the percentage of vertices on the liver mesh where the regression coefficients are statistically significant ($p < 0.05$) after adjustment for multiple comparisons. The total area has been split into areas of positive and negative associations.

| | Significance Area | $\hat{\beta} < 0$ | $\hat{\beta} > 0$ |
|---|---|---|---|
| Age | 57% | 18% | 39% |
| BMI | 87% | 54% | 33% |
| WHR | 55% | 29% | 26% |
| Liver Iron | 38% | 2% | 36% |
| Liver PDFF | 55% | 7% | 48% |

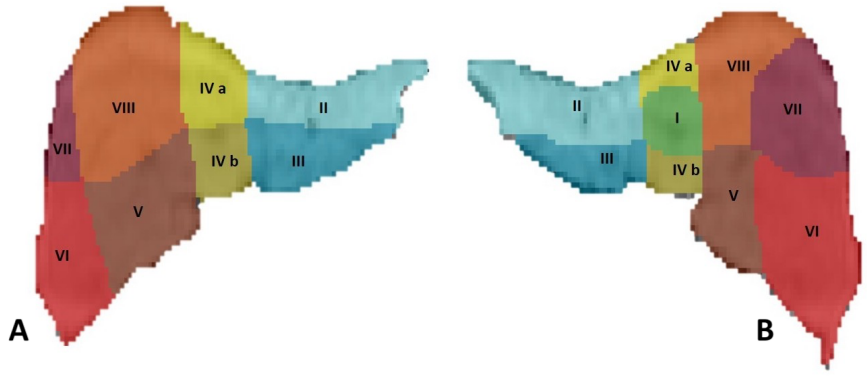


**Fig. 3.** Segments of the liver as described in the Couinaud classification, overlaid on the liver template. Projections are anterior (A) and posterior (B).

The Couinaud classification [11] of liver segments has been applied to the liver template for reference (Fig. 3). All the significant associations between S2S values and the three anthropometric covariates are shown in Fig. 4 and the association between S2S values and the liver IDPs are in Fig. 5. Interestingly, the statistical parametric maps with associations between S2S values and liver iron concentration and PDFF appear to show regional differences congruent with different segments of the liver proposed by Couinaud. Changes in liver morphology associated with liver PDFF appeared to be most pronounced in segments II & III and VI & VII, while changes in liver morphology associated with liver iron concentration were strongest in segments II & III. BMI and WHR were associated with the most pronounced positive S2S values in segments III & VI and part of IV & VII with negative S2S values in segments II & VIII.

## 4 Discussion and Conclusions

In this paper, we constructed surface meshes from liver segmentations of 2,730 subjects in the UK Biobank. Based on the vertices of the mesh, we were able to compute a 3D phenotype related to local shape variations and perform mass univariate regression analysis to model the associations with anthropometric and phenotypic traits.

We performed image registration and estimated a liver template with average shape using an optimal normalisation technique by computing the Euclidean mean of the of the non-rigid transformations. This normalization technique has been shown to provide the optimal mapping and template shape [3]. Also, the computation of the Euclidean mean has been shown to provide a good estimation of the template construction [5]. We used rigid registration to align the subject segmentations to the template in order to account for orientation and position differences obtaining a transformation in a standard space for each subject. There are a few ways of fixing these difference of the subjects' meshes. Previous studies investigating the shape and motion of the left ventricle of the heart removed these differences by retaining the shape and size for analysis [5,19].

Statistical parametric mapping has been a useful technique in neuroimaging [20] and cardiac imaging [9], showing that such statistical methods may be utilised in modelling the relationship between phenotypic and genetic variation [18]. Our findings demonstrate that the 3D mesh-derived phenotypes of the liver in specific anatomical regions are associated with the anthropometric/phenotypic traits using the SPM framework. We also found that liver IDPs were significantly associated with higher S2S values, suggesting that increased liver fat and iron concentration may have an impact on the liver shape and structure. It is also notable that the liver S2S values increase with age and waist-to-hip ratio. These findings agree with previous studies that report an increase in liver fat and iron is associated with predictors of metabolic disease [15]. Interestingly, the pattern of changes in S2S values across the liver reflect differences that might be attributed to different lobes and segments of the liver described in the Couinaud system of classification. Further work to explore this in more detail

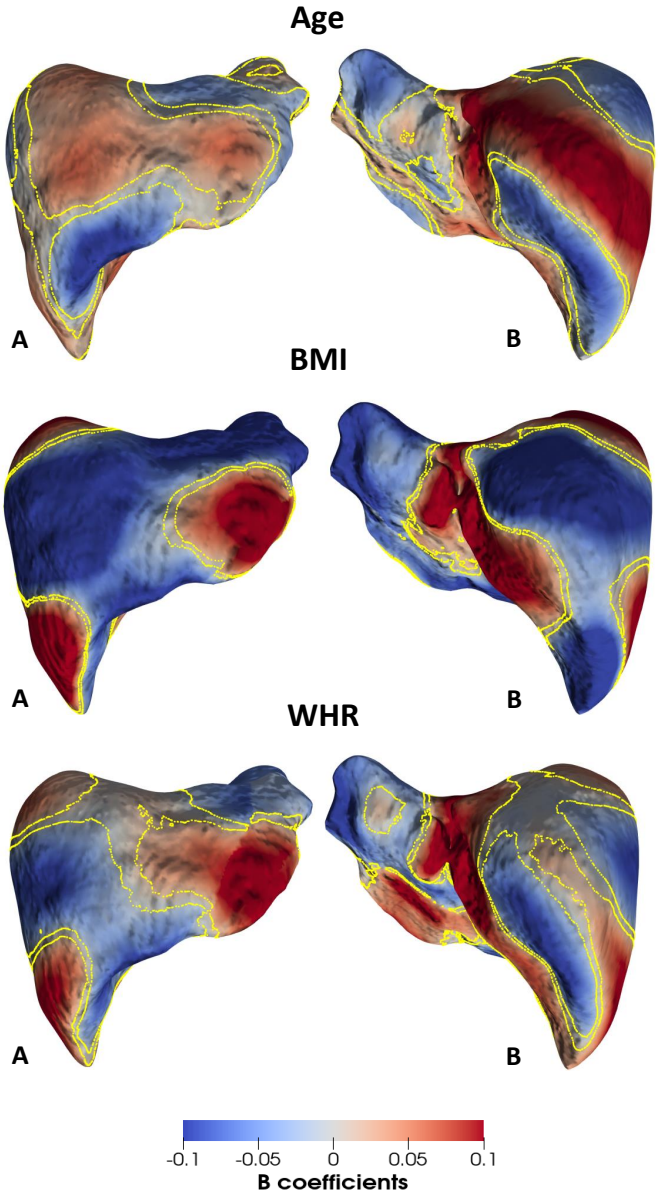


**Fig. 4.** Three-dimensional statistical parametric maps of liver morphology, projections are anterior (A) and posterior (B). The SPMs show the local strength of association between age, body mass index (BMI) and waist-to-hip ratio (WHR) with surface-to-surface values. Yellow contour lines indicate significant regions ($p < 0.05$) after correction for multiple testing, with positive associations in bright red and negative associations in bright blue.

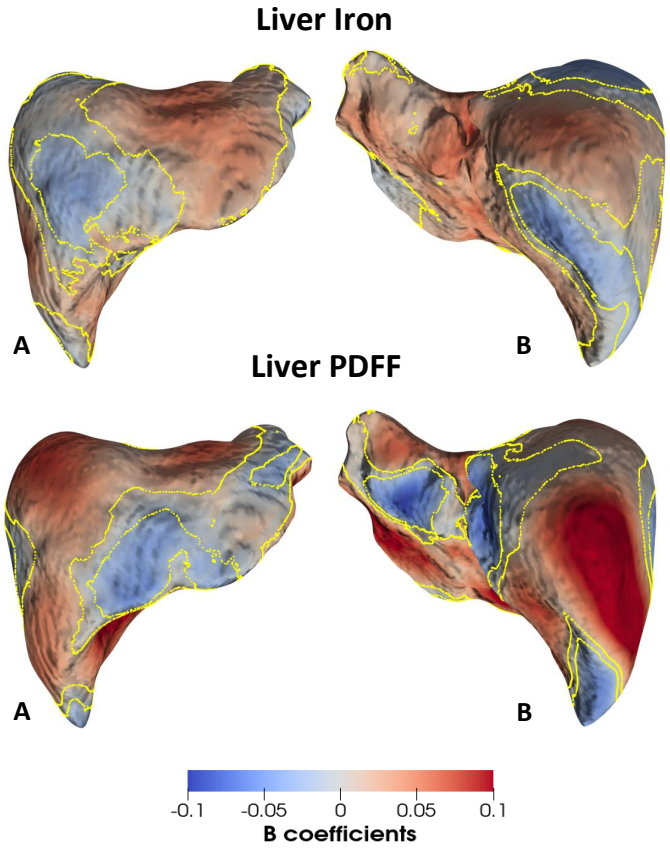


**Fig. 5.** Three-dimensional statistical parametric maps of liver morphology, projections are anterior (A) and posterior (B). The SPMs show the local strength of association between liver iron concentration and proton density fat fraction (PDFF) with surface-to-surface values. Yellow contour lines indicate significant regions ($p < 0.05$) after correction for multiple testing, with positive associations in bright red and negative associations in bright blue.

may allow further mapping the associations between genetic variations and 3D phenotypes in specific anatomical regions.

Organ shape variations could become a powerful tool for assessing global changes associated with organ damage (liver fibrosis and cirrhosis), disease progression and remission (fatty liver, haemochromatosis, nonalcoholic steatohepatitis) and eventually treatment outcome. Moreover, this technique has the potential to be simultaneously applied in multi-organ approaches (e.g., liver, pancreas, kidneys, spleen) thus giving a more holistic overview of health and disease than what is currently available from single-organ measurements. Future work will ap-

ply this method on a larger cohort as well as on other organs in the abdominal cavity, such as the pancreas, spleen and kidneys.

In conclusion, we have constructed a surface mesh of the liver anatomy in a sample of subjects from the UK Biobank population. From the surface mesh, we presented a 3D mesh-derived phenotype and were able to quantify the anatomical relationships with the anthropometric/phenotypic traits in the liver using the mass univariate regression analysis. We believe that the mesh construction and statistical techniques will benefit future research in population-based cohort studied, in identifying associations between physiological, genetic and anthropometric effects on liver structure and function as well as in other abdominal organs.

## 5 Acknowledgements

This research has been conducted using the UK Biobank Resource under Application Number '44584' and was funded by Calico Life Sciences LLC.

## References

1. Avants, B.B., Epstein, C., Grossman, M., Gee, J.C.: Symmetric diffeomorphic image registration with cross-correlation: Evaluating automated labeling of elderly and neurodegenerative brain. Medical Image Analysis **12**, 1361–8415 (2008). https://doi.org/10.1016/j.media.2007.06.004
2. Avants, B.B., Tustison, N.J., Song, G., Cook, P.A., Klein, A., Gee, J.C.: A reproducible evaluation of ANTs similarity metric performance in brain image registration. NeuroImage **54**, 2033–2044 (2011). https://doi.org/10.1016/j.neuroimage.2010.09.025
3. Avants, B.B., Yushkevich, E.P., Pluta, J., Minkoff, D., Korczykowski, M., Detre, J., Gee, J.C.: The optimal template effect in hippocampus studies of diseased populations. Neuroimage **49**, 2457–2466 (2010). https://doi.org/10.1016/j.neuroimage.2009.09.062
4. Bagur, A.T., Ridgway, G., McGonigle, J., Brady, M., Bulte, D.: Pancreas segmentation-derived biomarkers: Volume and shape metrics in the UK Biobank imaging study. In: Papież, B., Namburete, A., Yaqub, M., Noble, J. (eds.) Medical Image Understanding and Analysis. MIUA 2020. Communications in Computer and Information Science, vol. 1248, pp. 131–142. Springer, Cham (2020). https://doi.org/10.1007/978-3-030-52791-4_11
5. Bai, W., Shi, W., de Marvao, A., Dawes, T.J., O'Regan, D.P., Cook, S.A., Rueckert, D.: A bi-ventricular cardiac atlas built from 1000+ high resolution MR images of healthy subjects and an analysis of shape and motion. Medical Image Analysis **26**(1), 133–145 (2015). https://doi.org/10.1016/j.media.2015.08.009
6. Benjamini, Y., Hochberg, Y.: Controlling the false discovery rate: A practical and powerful approach to multiple testing. Methodological **57**, 289–300 (1995). https://doi.org/10.1111/j.2517-6161.1995.tb02031.x
7. Beygelzimer, A., Kakadet, S., Langford, J., Arya, S., Moun, D., Li, S.: Fast Nearest Neighbor Search Algorithms and Applications (2019), https://rdrr.io/cran/FNN, R package version 1.1.3

8. Biffi, C.: An introduction to mass univariate analysis of three-dimensional phenotypes (2017), https://github.com/UK-Digital-Heart-Project/mutools3D, R package version 1.0
9. Biffi, C., de Marvao, A., Attard, M.I., Dawes, T.J.W., Whiffin, N., Bai, W., Shi, W., Francis, C., Meyer, H., Buchan, R., Cook, S.A., Rueckert, D., O'Regan, D.P.: Three-dimensional cardiovascular imaging-genetics: A mass univariate framework. Bioinformatics **34**, 97–103 (2018). https://doi.org/10.1093/bioinformatics/btx552
10. Bycroft, C., Freeman, C., Petkova, D., Band, G., Elliott, L.T., Sharp, K., Motyer, A., Vukcevic, D., Delaneau, O., O'Connell, J., Cortes, A., Welsh, S., Young, A., Effingham, M., McVean, G., Leslie, S., Allen, N., Donnelly, P., Marchini, J.: The UK biobank resource with deep phenotyping and genomic data. Nature **562**(7726), 203–209 (2018). https://doi.org/10.1038/s41586-018-0579-z
11. Couinaud, C.: Le Foie: Études Anatomiques et Chirurgicales. Masson, Paris (1957)
12. Dixon, W.T.: Simple proton spectroscopic imaging. Radiology **153**(1), 189–194 (1984). https://doi.org/10.1148/radiology.153.1.6089263
13. Freedman, D., Lane, D.: A nonstochastic interpretation of reported significance levels. Journal of Business & Economic Statistics **1**, 292–298 (1983). https://doi.org/10.1080/07350015.1983.10509354
14. Guillaume, B., Wang, C., Poh, J., Shen, M.J., Ong, M.L., Tan, P.F., Karnani, N., Meaney, M., Qiu, A.: Improving mass-univariate analysis of neuroimaging data by modelling important unknown covariates: Application to epigenome-wide association studies. NeuroImage **173**, 57–71 (2018). https://doi.org/10.1016/j.neuroimage.2018.01.073
15. Kühn, J.P., Meffert, P., Heske, C., Kromrey, M.L., Schmidt, C.O., Mensel, B., Völzke, H., Lerch, M.M., Hernando, D., Mayerle, J., Reeder, S.B.: Prevalence of fatty liver disease and hepatic iron overload in a Northeastern German population by using quantitative MR imaging. Radiology **284**, 706–716 (2017). https://doi.org/10.1148/radiol.2017161228
16. Littlejohns, T.J., Holliday, J., Gibson, L.M., Garratt, S., Oesingmann, N., Alfaro-Almagro, F., Bell, J.D., Boultwood, C., Collins, R., Conroy, M.C., Crabtree, N., Doherty, N., Frangi, A.F., Harvey, N.C., Leeson, P., Miller, K.L., Neubauer, S., Petersen, S.E., Sellors, J., Sheard, S., Smith, S.M., Sudlow, C.L.M., Matthews, P.M., Allen, N.E.: The UK Biobank imaging enhancement of 100,000 participants: Rationale, data collection, management and future directions. Nature Communications **11**(1), 1–12 (2020). https://doi.org/10.1038/s41467-020-15948-9
17. Liu, Y., Basty, N., Whitcher, B., Bell, J.D., Sorokin, E., van Bruggen, N., Thomas, E.L., Cule, M.: Genetic architecture of 11 abdominal organ traits derived from abdominal MRI using deep learning. eLife (2021), in press.
18. de Marvao, A., McGurk, K.A., Zheng, S.L., Thanaj, M., Bai, W., Duan, J., Biffi, C., Mazzarotto, F., Statton, B., Dawes, T.J., Savioli, N., Halliday, B.P., Xu, X., Buchan, R.J., Baksi, A.J., Quinlan, M., Tokarczuk, P., Tayal, U., Francis, C., Whiffin, N., Theotokis, P.I., Zhang, X., Jang, M., Berry, A., Pantazis, A., Barton, P.J., Rueckert, D., Prasad, S.K., Walsh, R., Ho, C.Y., Cook, S.A., Ware, J.S., O'Regan, D.P.: Outcomes and phenotypic expression of rare variants in hypertrophic cardiomyopathy genes amongst UK Biobank participants. medRxiv (2021). https://doi.org/10.1101/2021.01.21.21249470
19. Medrano-Gracia, P., Cowan, B.R., Ambale-Venkatesh, B., Bluemke, D.A., Eng, J., Finn, J.P., Fonseca, C.G., Lima, J.A.C., Suinesiaputra, A., Young, A.A.: Left ventricular shape variation in asymptomatic populations: the multi-ethnic study of atherosclerosis. Journal of Cardiovascular Magnetic Resonance **16**, 56 (2014). https://doi.org/10.1186/s12968-014-0056-2

20. Penny, W., Friston, K., Ashburner, J., Kiebel, S., Nichols, T.: Statistical Parametric Mapping: The Analysis of Functional Brain Images. Elsevier/Academic Press, Amsterdam, Boston (2007). https://doi.org/10.1016/B978-0-12-372560-8.X5000-1
21. R Core Team: R: A Language and Environment for Statistical Computing. R Foundation for Statistical Computing, Vienna, Austria (2020), https://www.R-project.org
22. Ronneberger, O., Fischer, P., Brox, T.: U-net: Convolutional networks for biomedical image segmentation. In: Navab, N., Hornegger, J., Wells, W., Frangi, A. (eds.) Medical Image Computing and Computer-Assisted Intervention – MICCAI 2015. Lecture Notes in Computer Science, vol. 9351, pp. 234–241. Springer, Cham (2015). https://doi.org/10.1007/978-3-319-24574-4_28
23. Schlager, S., Francois, G.: Manipulations of Triangular Meshes Based on the 'VCGLIB' API (2021), https://github.com/zarquon42b/Rvcg, R package version 0.19.2
24. Smith, S.M., Nichols, T.E.: Threshold-free cluster enhancement: Addressing problems of smoothing, threshold dependence and localisation in cluster inference. NeuroImage **4**, 83–98 (2009). https://doi.org/10.1016/j.neuroimage.2008.03.061
25. Thomas, E.L., Fitzpatrick, J., Frost, G.S., Bell, J.D.: Metabolic syndrome, overweight and fatty liver. In: Berdanier, C., Dwyer, J., Heber, D. (eds.) Handbook of Nutrition and Food, pp. 763–768. CRC Press, Boca Raton, USA, 3 edn. (2013). https://doi.org/10.1201/b15294
26. Winkler, A.M., Ridgway, G.R., Webster, M.A., Smith, S.M., Nichols, T.E.: Permutation inference for the general linear model. NeuroImage **92**, 381–397 (2014). https://doi.org/10.1016/j.neuroimage.2014.01.060
27. Younossi, Z.M.: Non-alcoholic fatty liver disease - A global public health perspective. Journal of Hepatology **70**(3), 531–544 (2019). https://doi.org/10.1016/j.jhep.2018.10.033